Supporting Information

High-Performance Nitrogen-doped Intermetallic PtNi Catalyst for the Oxygen Reduction Reaction

Xueru Zhao [a,b], Cong Xi [b], Rui Zhang [c], Liang Song [a], Chenyu Wang [d], Jacob S. Spendelow [d], Anatoly I. Frenkel [a,e], Jing Yang [b,*], Huolin L. Xin [c,*], and Kotaro Sasaki [a,*]

[a] *Chemistry Department, Brookhaven National Laboratory, Upton, NY, 11973, USA*

[b] *Institute of New-Energy Materials, Key Laboratory of Advanced Ceramics and Machining Technology of Ministry of Education, School of Materials Science and Engineering, Tianjin University, Tianjin, 300072, China*

[c] *Department of Physics and Astronomy, University of California, Irvine, CA, 92697, USA*

[d] *Materials Physics and Application Division, Los Alamos National Laboratory, Los Alamos, NM, 87545, USA*

[e] *Department of Materials Science and Chemical Engineering, Stony Brook University, Stony Brook, NY, 11794, USA*

* Corresponding authors.

E-mail addresses: yang_jing@tju.edu.cn (J. Yang), huolinx@uci.edu (H. L. Xin), ksasaki@bnl.gov (K. Sasaki).

Experimental Details

Materials and Chemicals

The Ketjenblack (KB) EC300J carbon was purchased from Akzo Nobel Surface Chemical LLC. Nickel(II) acetylacetonate ($Ni(acac)_2$, 95 %), and platinum(II) acetylacetonate ($Pt(acac)_2$, 98%) were purchased from Sigma-Aldrich. Acetone (CH_3OCH_3, HPLC) and iso-propanol (IPA, HPLC) were purchased from Spectrum Chemical MFG Group and Sigma-Aldrich, respectively. All aqueous solutions/suspensions used in this study were prepared using Millipore ultrapure (18.2 MΩ·cm) water. Ar (99.999%), O_2 (99.6%), CO (99.99%), H_2 (99%, extra dry) and anhydrous ammonia (NH_3) gases were purchased from Praxair Inc. Commercial Pt/C (TEC10E50E, Pt 46.4 wt %) was purchased from Tanaka Kikinzoku Kogyo (TKK) Corp.

Synthesis of catalysts

The Int-PtNiN/KB catalysts were synthesized as follows: 330 mg of $Pt(acac)_2$, 200 mg $Ni(acac)_2$ and 500 mg of KB were dispersed in 80 mL of acetone, and then sonicated for 30 min. The suspension was kept at room temperature with magnetic stirring for 1 h. Then the mixture was dried by a rotating evaporator device. The dried precursor was then annealed at 560 °C for 9 h in a tube furnace under flowing NH_3 to form an ordered intermetallic phase. The inductively coupled plasma (ICP) analysis showed that the resultant Int-PtNiN/KB catalyst has 18.3 wt% Pt.

For comparison, disordered PtNiN/KB (D-PtNiN/KB) and disordered PtNi/KB (D-PtNi/KB) were prepared by the similar procedure. D-PtNiN/KB was obtained by

annealing at 560 °C for 2 h under flowing NH_3. And D-PtNi/KB was obtained by annealing at 560 °C for 9 h under flowing H_2/Ar (5 % H_2).

Materials characterization

Transmission electron microscopy (TEM), High-angle annular dark-field scanning transmission electron microscopy (HAADF-STEM), and energy dispersive X-ray spectroscopy (EDX) elemental mapping images were obtained by FEI Tecnai F20 TEM at an accelerating voltage of 200 kV. X-ray powder diffraction (XRD) patterns were collected on a Mar345 image plate detector with Cu-Kα radiation.

In situ X-ray absorption spectroscopy (XAS) measurements using an electrochemical cell were carried out at the QAS beamline (7-ID) of the National Synchrotron Light Source II (NSLS II) at Brookhaven National Laboratory (BNL). The catalyst sample (working electrode), a proton exchange membrane (Nafion 117, DuPont Chemical Co., DE) and a Pt thin foil (counter electrode) were sandwiched and clamped tightly by the two acrylic plastic bodies. Each plastic body has an X-ray window. The electrolyte was 1 M $HClO_4$ and a Ag/AgCl leak-free electrode was used as a reference electrode. Details of the electrochemical cell are given elsewhere.[1] The XAS data were processed and analyzed by Athena and Artemis software.[2]

Electrochemical measurements

A glassy carbon ring disk electrode (RDE) with an area of 0.196 cm^2 was the working electrode, which was polished with 0.3 μm and 0.05 μm alumina slurry to obtain a mirror-like surface. A Pt wire was the counter electrode and a leak-free Ag/AgCl electrode was the reference electrode. The catalyst ink was prepared by ultrasonic mixing

of 5 mg of the catalyst with 4 mL Milli-Q water, 1 mL iso-propanol and 5 μL 10 wt% Nafion solution until a uniform ink was obtained. 10 μL of this ink was deposited onto the glassy carbon RDE and dried in air at room temperature. The total loading of Pt was used to calculate the mass activity. All the potentials are reported with respect to a reversible hydrogen electrode (RHE). The cyclic voltammetry (CV) characterization of the catalysts was carried out in an Ar-purged 0.1 M $HClO_4$ aqueous solution at a scan rate of 20 mV s^{-1}. The linear scanning voltammetry (LSV) for the ORR was obtained in O_2-saturated 0.1 M $HClO_4$ solution by scanning the potential from 0 to 1.1 V versus RHE (scan rate: 10 mV s^{-1}; rotation rate: 400, 625, 900, 1225, 1600, and 2025 rpm). Stability tests for the catalyst were conducted in air-saturated 0.1 M $HClO_4$ in the potential range from 0.6 to 0.95 V at a sweep rate of 100 mV s^{-1} at room temperature. For comparison, the commercial Pt/C, D-PtNi/KB and D-PtNiN/KB catalysts were tested under the same measuring conditions.

The Koutecky-Levich equation can be described as follows:

$$\frac{1}{i} = \frac{1}{i_L} + \frac{1}{i_K} = \frac{1}{B\omega^{1/2}} + \frac{1}{i_K} \quad \ldots\ldots$$

where i, i_L, and i_K represent the measured, diffusion-limited, and kinetic current density, respectively. B is a constant and w is the rotation rate.

MEA preparation and fuel cell tests

As-synthesized Int-PtNiN/KB catalyst was incorporated into the membrane electrode assembly (MEA) by direct spraying of a water/n-propanol based ink onto a Nafion 211 membrane. The MEA was prepared with a Pt loading of 0.121 mg_{Pt} cm^{-2} on the cathode side. H_2-air fuel cell testing was carried out in a single cell using a commercial fuel cell

test system (Fuel Cell Technologies Inc.). The MEA was sandwiched between two graphite plates with straight parallel flow channels machined in them. The cell was operated at 80 °C, with 150 kPa_{abs} H_2/air or H_2/O_2, and a gas flow rate of 500/1000 sccm for anode/cathode, respectively. Catalyst mass activity was measured via the current DOE/FCTT protocol (potential step from 0.6 V to 0.9 V and 15 min hold, current averaged during last 1 min) and by measuring the current at 0.9 V (*iR*-free) in 150 kPa_{abs} H_2/O_2 (80 °C, 100 % relative humidity (RH), 500/1000 sccm) with correction for measured H_2 crossover. The electrochemical active surface area was obtained by calculating underpotentially-deposited hydrogen (H_{UPD}) charge in CV curves between 0.1-0.4 V (0.45-0.55 V background subtracted); assuming a value of 210 μC/cm^2 for the adsorption of a hydrogen monolayer on Pt (CV curves were obtained under 150 kPa_{abs} H_2/N_2, 30 °C, > 100 % RH, 500/1000 sccm). The potential cycling accelerated durability test (ADT) was conducted by using the trapezoidal wave method from 0.6 V to 0.95 V with 0.5 s rise time and 2.5 s hold time (150 kPa_{abs} H_2/N_2, 80 °C, 100 % RH, 200/200 sccm).

DFT Calculations Details

The DFT calculations were carried out on a Pt (111) surface of ordered PtNi to explore the influence of lattice tensile on ORR properties in acid environment by the Vienna Ab initio Simulation Package (VASP).[3-4] The projector augmented wave (PAW) potentials were employed to describe the nuclei-electron interactions.[5] The generalized gradient approximation (GGA)[6] with the Perdew-Burke-Ernzerhof (PBE)[7] functional was used to describe the electron exchange-correlation interactions. Spin polarization was considered throughout the calculations. The wave functions of valence electrons were expanded by

plane wave basis set with a cut off energy of 500 eV. The convergence criteria for energy and force during geometrical optimization were set to 10^{-6} eV and 0.03 eV/A˚, respectively. The vacuum space of 15 A˚ was applied to avoid the interactions along the z-direction. The Brillouin zone was sampled by a 5 ×5 × 1 Monkhorst-Pack mesh grid. The 2 × 2 metal surface was simulated with six Pt atomic layers with the two bottom layers fixed and the top four layers allowed to fully relax to simulate the reaction of the interface atoms. The 50 % of Pt in the bottom three layers was uniformly substituted by Ni atoms along the y axis. The tensile strain by N-doping was applied by expanding the lattice length in x and y direction in the Pt(111) surface of the ordered PtNi.

The adsorption energy (E_X^{ads}) of each intermediate was calculated by the following equation:

$$E_X^{ads} = E_{*X} - E_* - E_X$$

where E_{*X} , E_* and E_X are energies of Pt-Ni(111) surface with intermediate, clean Pt-Ni (111) surface, and each intermediate.

The Gibbs free energy (G) of the adsorbed intermediate was calculated by

$$G = E_{DFT} + ZPE - TS$$

where E_{DFT} is the total electronic energy obtained with DFT, ZPE is the zero-point energy correction and S is the entropy of the system obtained through vibrational frequency analysis.

Supplementary Figures

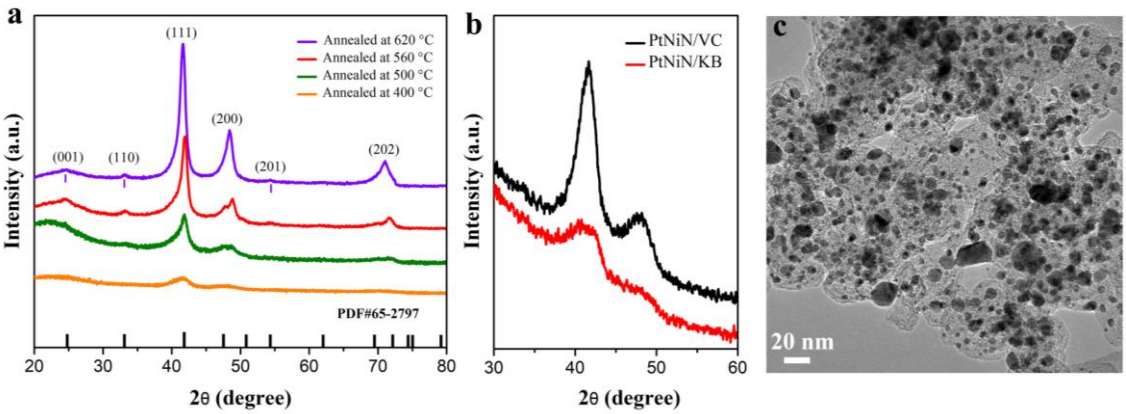

Figure S1. (a) XRD patterns of PtNiN/KB samples annealed at different temperatures for 9 h. (b) XRD patterns of PtNiN/VC (Vulcan XC72R) and PtNiN/KB synthesized by annealing at 510°C for 2 h in an NH_3 gas. The particle sizes calculated by the Scherrer equation are 3.9 and 1.7 nm for PtNiN/VC and PtNiN/KB, respectively. (c) The TEM image of PtNiN/KB samples annealed at 620 °C for 9h.

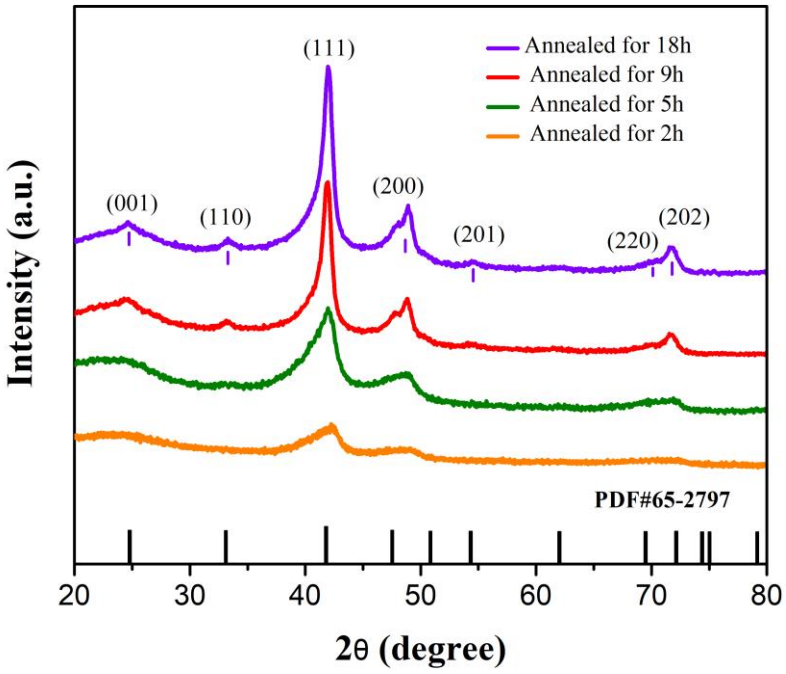

Figure S2. XRD patterns of PtNiN/KB samples annealed at 560 °C for different annealing time.

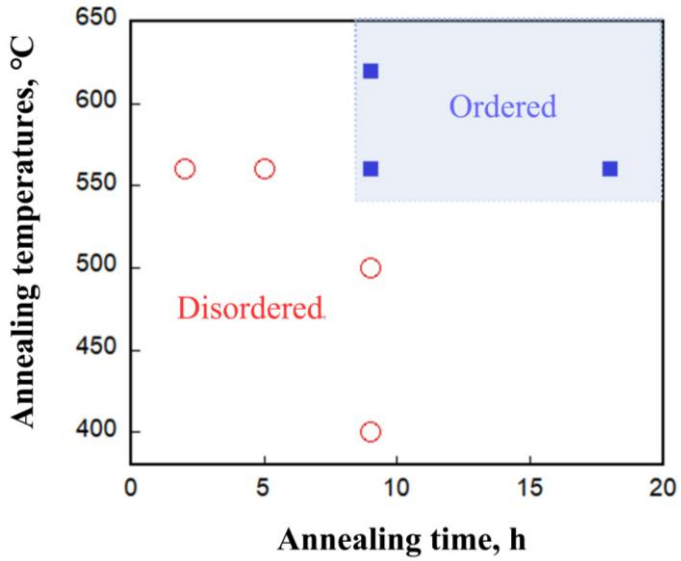

Figure S3. Time-temperature-transformation (TTT) diagram of the PtNiN system based on the data in Figure S1 and S2.

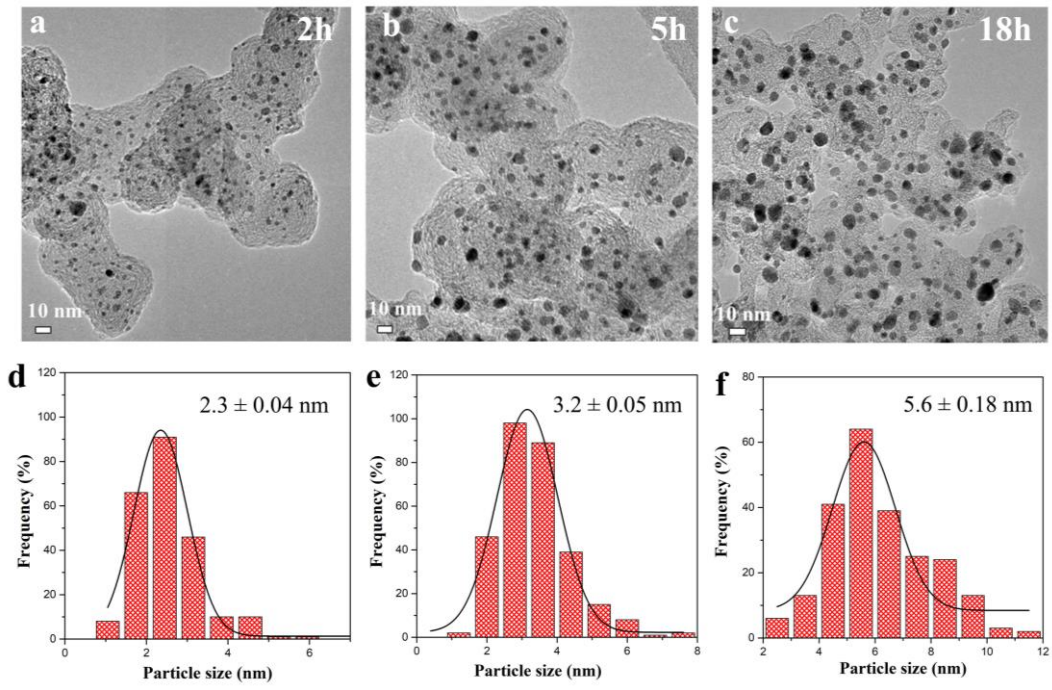

Figure S4. Overview of PtNiN/KB nanoparticles distribution on KB annealed at different time (a) 2h, (b) 5h and (c) 18h. The particle size of PtNiN/KB nanoparticles annealed at different time (d)

2h, (e) 5h and (f) 18h, obtained from the fitted profile (Gaussian distribution).

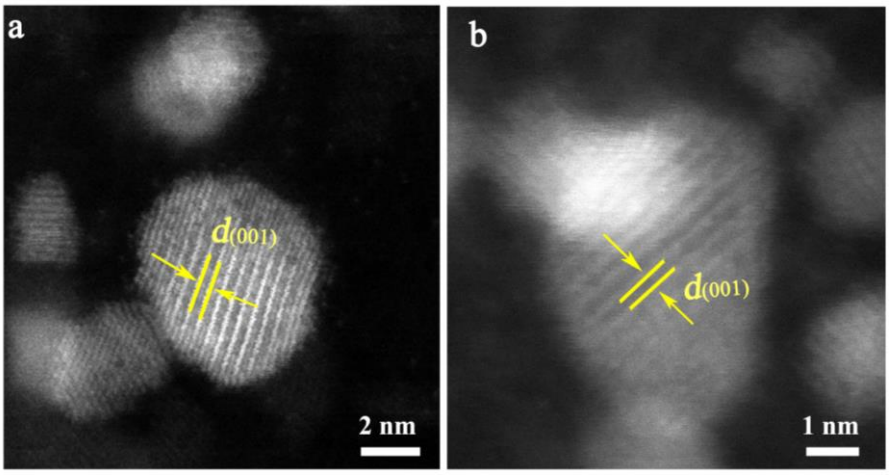

Figure S5. HADDF-STEM images of Int-PtNiN/KB sample.

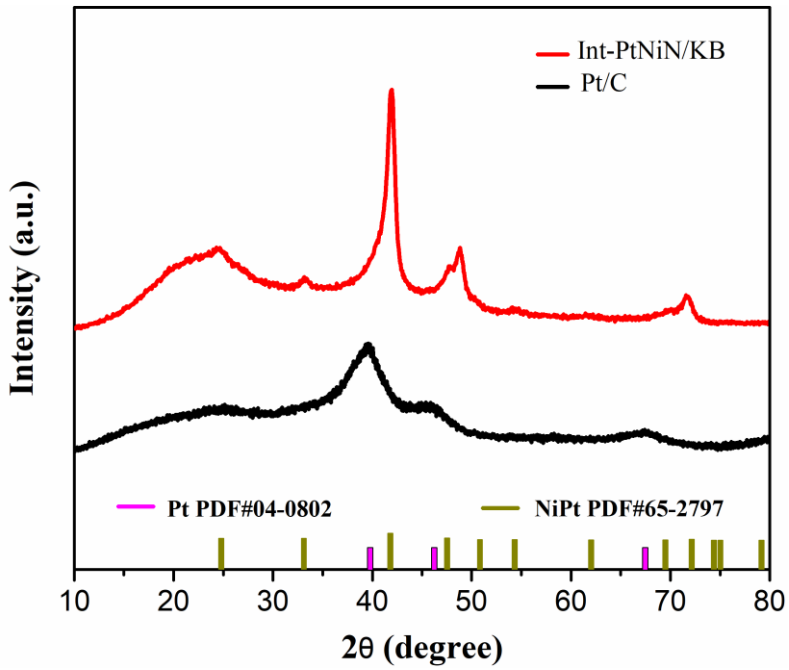

Figure S6. XRD patterns of Int-PtNiN/KB and Pt/C samples

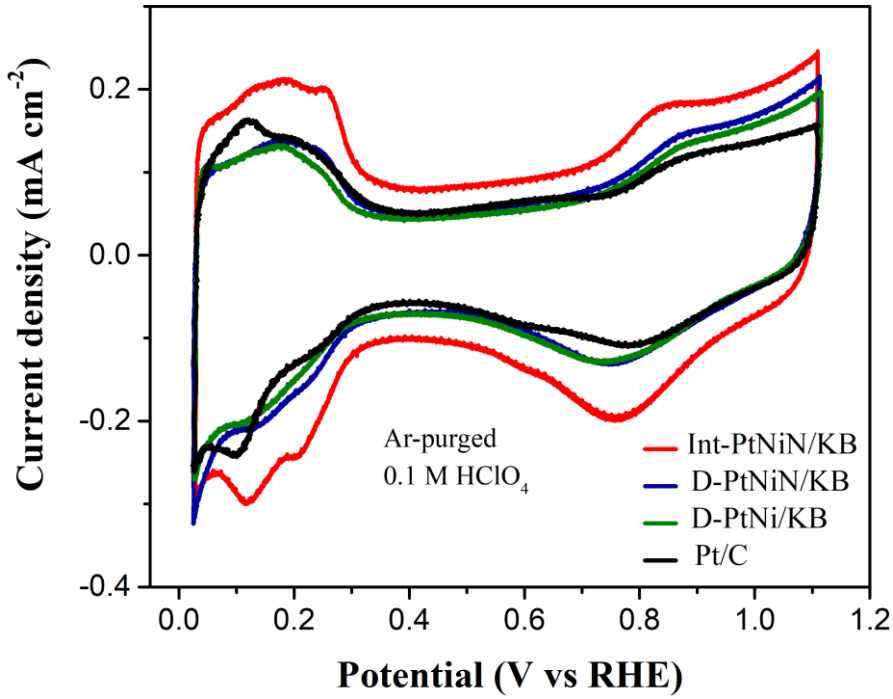

Figure S7. CV curves of Int-PtNiN/KB, D-PtNiN/KB, D-PtNi/KB and commercial Pt/C in Ar-purged 0.1 M $HClO_4$ solution (20 mV s^{-1}).

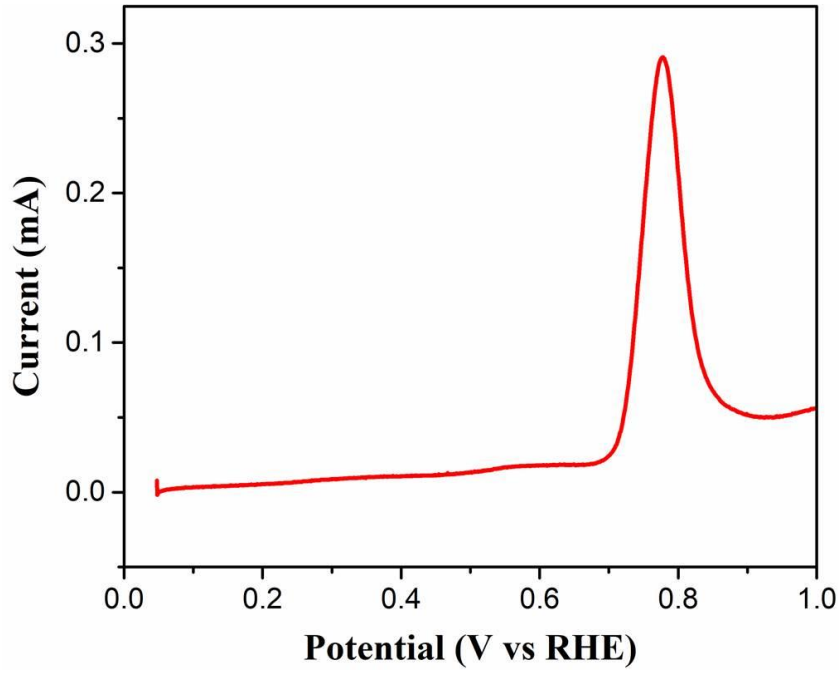

Figure S8. CO stripping curve of Int-PtNiN/KB catalyst obtained in 0.1 M $HClO_4$ bubbled with CO at a scan rate of 20 mV s^{-1}.

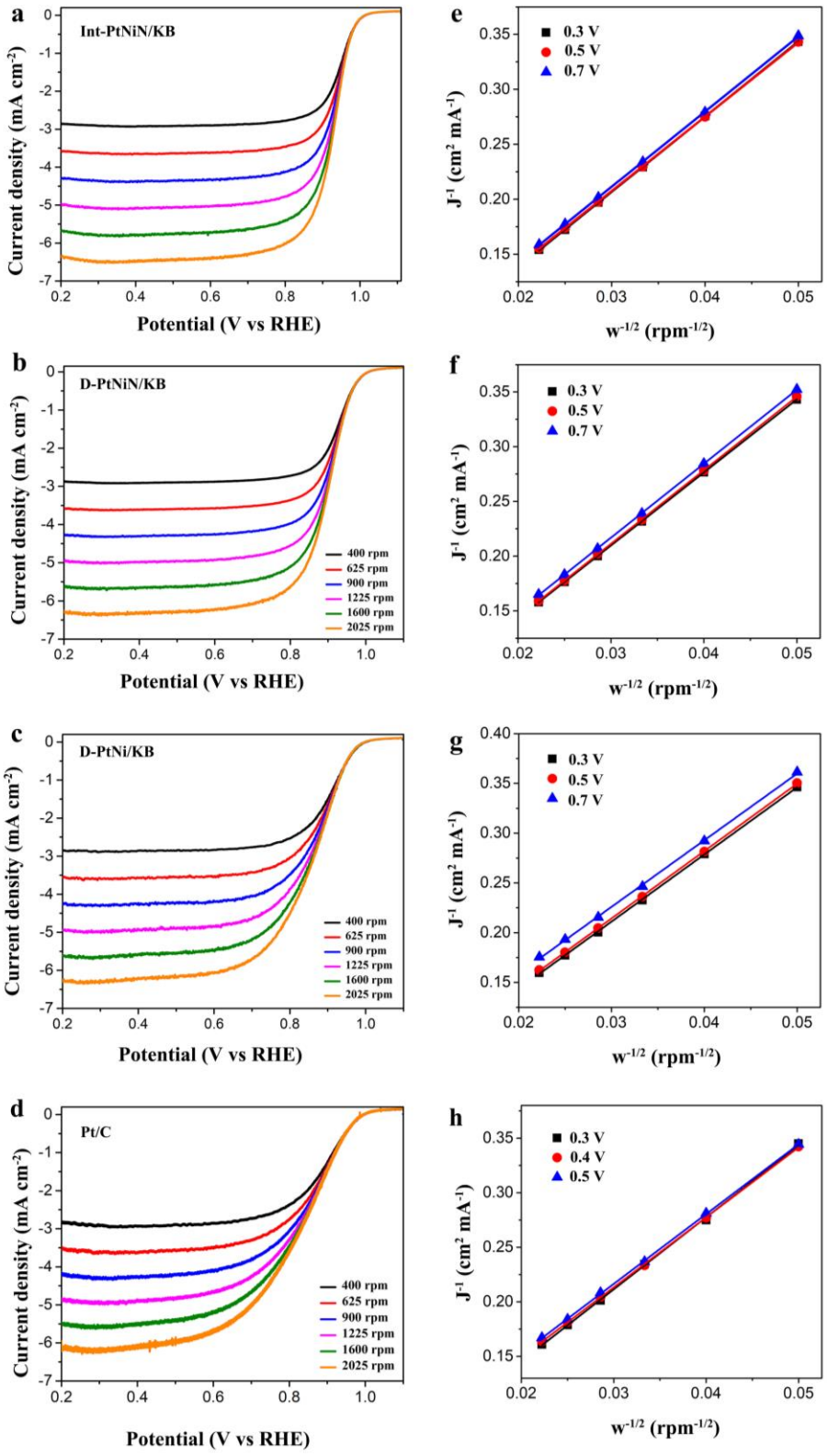

Figure S9. ORR polarization curves of (a) Int-PtNiN/KB, (b) D-PtNiN/KB, (c) D-PtNi/KB and (d) Pt/C in O_2-saturated 0.1 M $HClO_4$ at various rotation speeds and the corresponding Koutecky-Levich plots at different potentials (e-h).

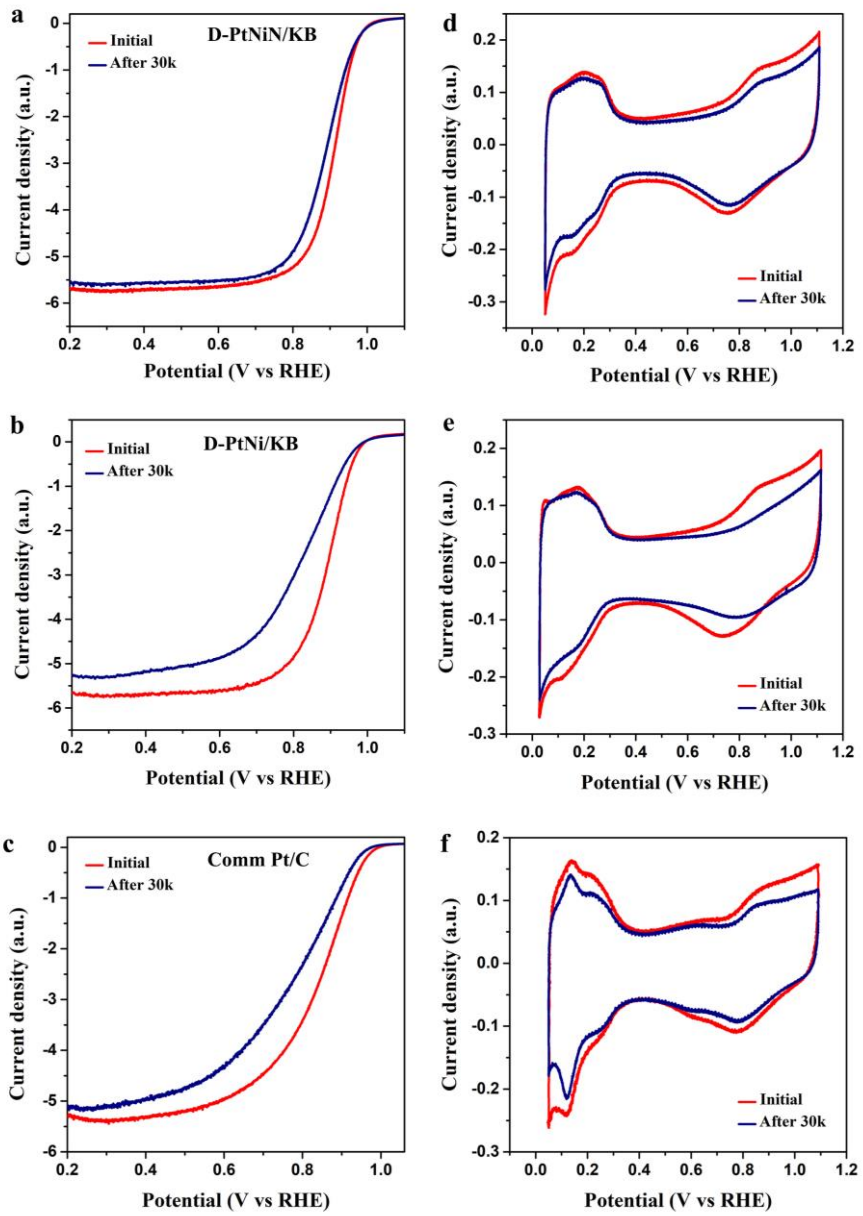

Figure S10. ORR polarization curves of (a) D-PtNiN/KB, (b) D-PtNi/KB, and (c) Pt/C before and after ADT 30,000 cycles. CV curves of (d) D-PtNiN/KB, (e) D-PtNi/KB, and (f) Pt/C before and after ADT 30,000 cycles. Notes: The ORR polarization curves were collected by using LSV method in O_2-saturated 0.1 M $HClO_4$ with a scanning rate of 10 mV s^{-1}. The CV curves were collected in Ar-saturated 0.1 M $HClO_4$ with a scanning rate of 20 mV s^{-1}. The durability tests of all catalysts were conducted by cycling the potential between 0.6 and 0.95 V at a scanning rate of 100 mV s^{-1} in 0.1 M $HClO_4$ bubbled with air.

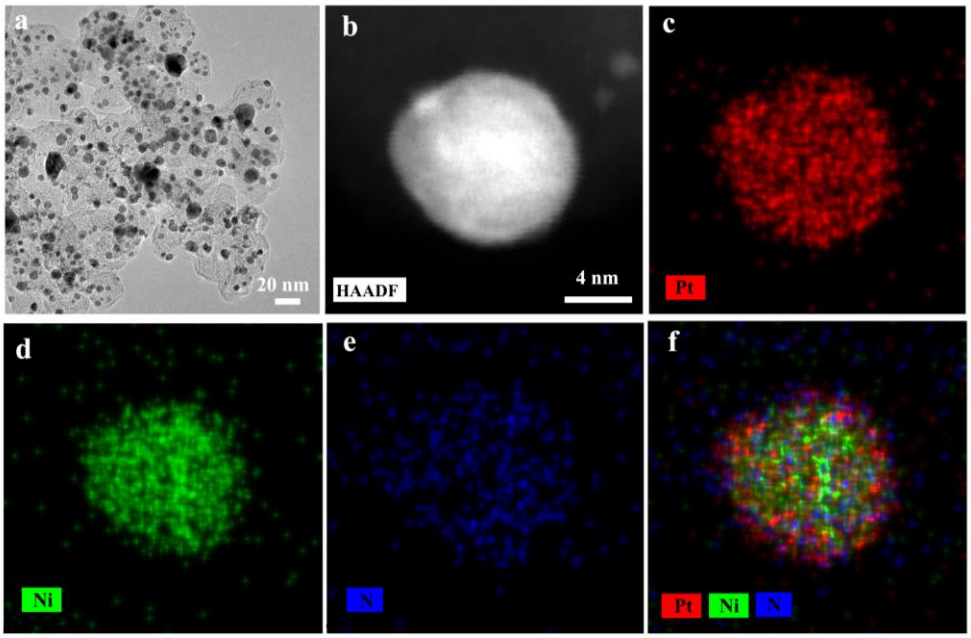

Figure S11. (a) TEM image of Int-PtNiN/KB catalyst after ADT 30,000 cycles. (b-f) HAADF-STEM and EDX elemental mapping of Int-PtNiN/KB after ADT 30,000 cycles.

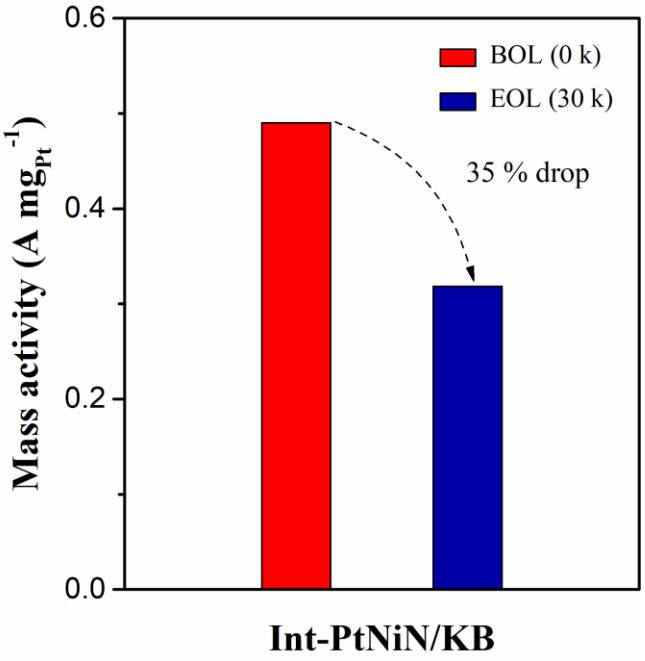

Figure S12. Mass activities of Int-PtNiN/KB collected at BOL and EOL (30,000 cycles) of MEA tests via the current DOE/fuel cell technologies team protocol (potential step from 0.6 to 0.9 V and 15 min hold, current averaged during last 1 min), and by measuring the current at 0.9 V (*iR*-free) in 150 kPa_{abs} H_2/O_2 (80 °C, 100% RH) with correction for measured H_2 crossover.

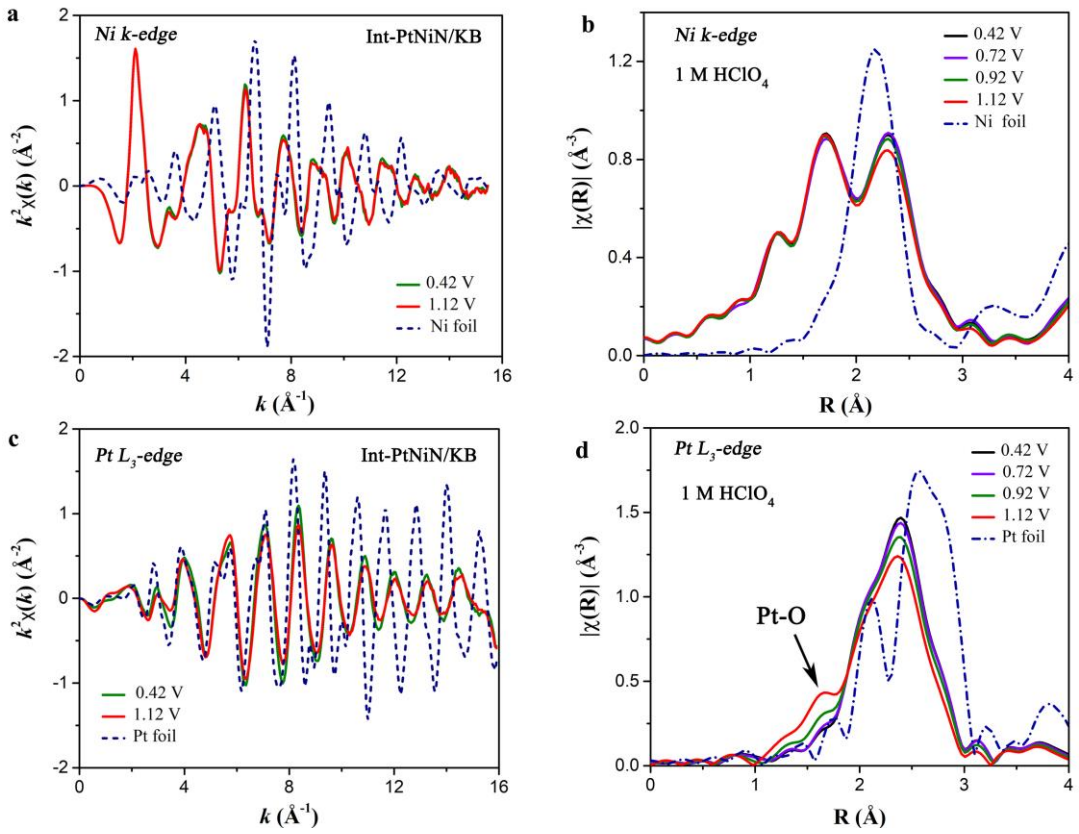

Figure S13. *In situ* Ni K-edge (a) *k*-space (k^2-weighted) EXAFS and (b) FT-EXAFS spectra of Int-PtNiN/KB at different potentials with those of a Ni reference foil. *In situ* Pt L_3-edge (c) *k*-space (k^2-weighted) EXAFS and (d) FT-EXAFS spectra of Int-PtNiN/KB with those of a Pt reference foil. The *in situ* data were collected in 1 M $HClO_4$.

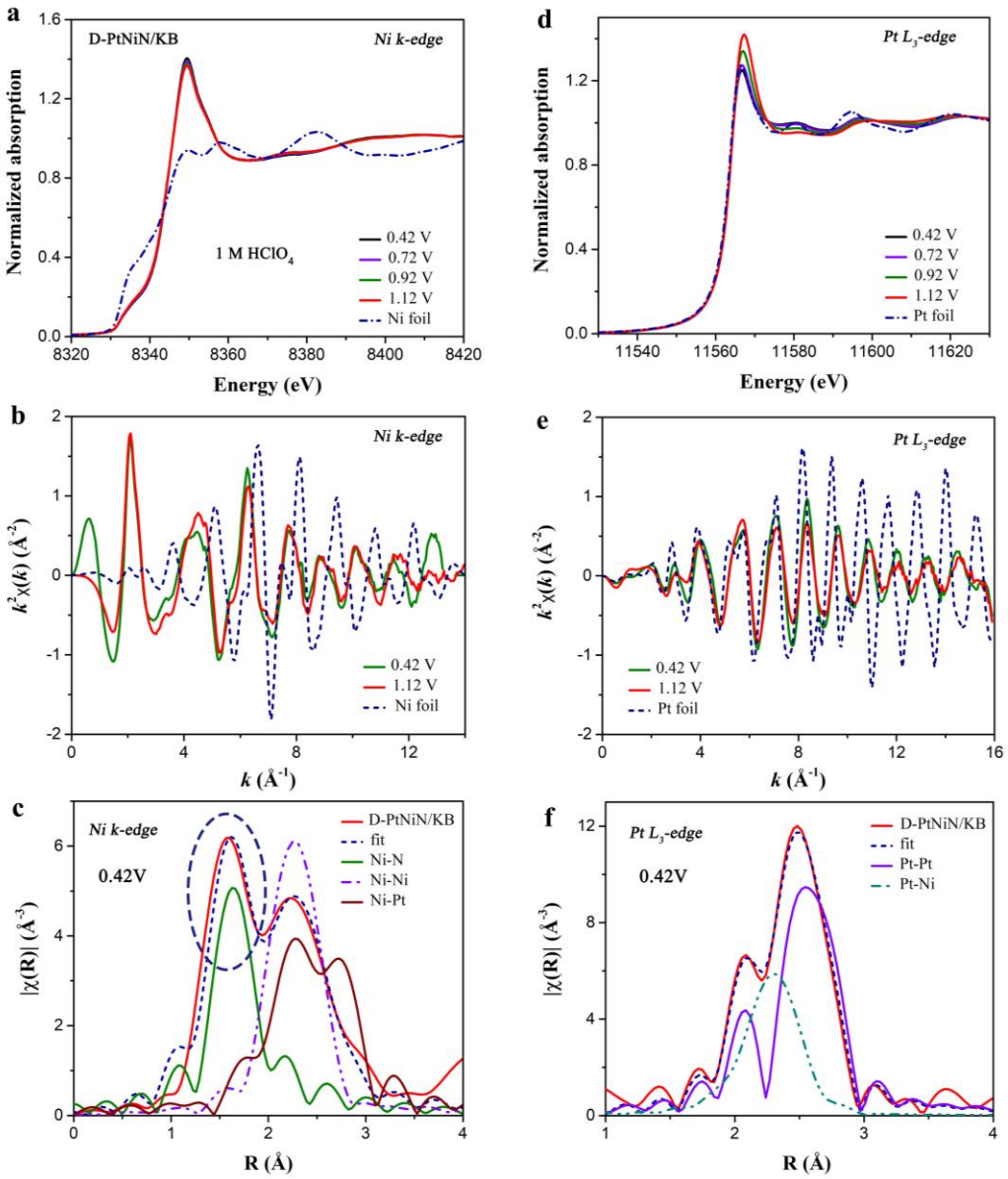

Figure S14. *In situ* Ni K-edge (a) XANES, (b) *k*-space (k^2-weighted) EXAFS at different potentials with those of a Ni reference foil, and (c) FT-EXAFS at 0.42 V with a first-shell fit together with Ni-Ni, Ni-Pt, and Ni-N contributions of D-PtNiN/KB. *In situ* Pt L_3-edge (d) XANES, (e) *k*-space (k^2-weighted) EXAFS at different potentials with those of a Pt reference foil, and (f) FT-EXAFS at 0.42 V with a first-shell fit together with Pt-Pt and Pt-Ni contributions of D-PtNiN/KB. The *in situ* data were collected in 1 M $HClO_4$.

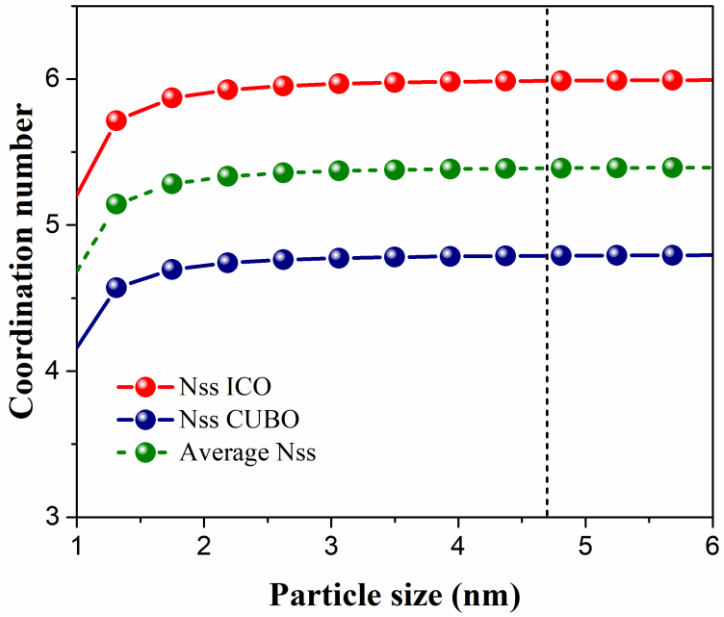

Figure S15. Coordination numbers of surface atoms (N_{ss}) for icosahedrons (ICO) and cuboctahedrons (CUBO) calculated from a theoretical nanocluster model.[8] The particle sizes were calculated from a volume-correlated sphere model using an average diameter d = 0.265 nm.[9]

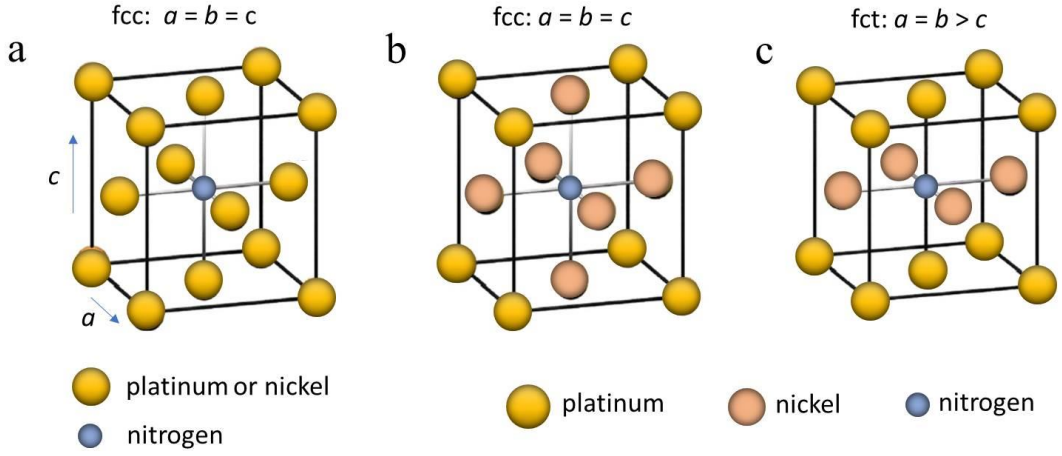

Figure S16. PtNiN atomic models of (a) Pt and Ni atoms occupying at fcc sites randomly with a nitrogen atom at a center of fcc, (b) Pt sited at corners and Ni sited at face centers with a nitrogen atom at a center of fcc (N of Ni-N is 6), and (c) a $L1_0$-type structure with a nitrogen atom at a center of fct (N of Ni-N is 4).

Supplementary Tables

Table S1. XRD results of Pt/C, D-PtNi/KB, D-PtNiN/KB and Int-PtNiN/KB.

Catalysts	Lattice constant, nm a*, b*	Lattice constant, nm c*	Strain (a*, b*)%	Strain (c*)%
Pt/C	0.3937	0.3937	----	----
D-PtNi/KB	0.3715	0.3715	5.88	5.88
D-PtNiN/KB	0.3736	0.3736	5.09	5.09
Int-PtNiN/KB	0.3746	0.3690	4.84	6.27

Compressive strains are calculated by $\varepsilon_{a^*}=(a_{Pt}-a^*)/a_{Pt}$, where a_{Pt} is the lattice constant of Pt/C, a*, b* and c* indicates the lattice constant in a unit cell along the x, y and z.

Table S2. The half-wave potential ($E_{1/2}$), MA, ECSA, and SA of Int-PtNiN/KB, D-PtNiN/KB, D-PtNi/KB and commercial Pt/C catalysts determined by RDE measurements

Catalysts	$E_{1/2}$ (mV)	MA @ 0.9 V (A mg_{Pt}^{-1})	ECSA (m^2 g^{-1})	SA @ 0.9 V (mA cm^{-2})
Int-PtNiN/KB	935	1.83	62.6	2.92
D-PtNiN/KB	908	0.58	46.3	1.25
D-PtNi/KB	890	0.46	42.0	1.10
PtC	850	0.18	46.9	0.38

Table S3. The half-wave potential ($E_{1/2}$), MA, ECSA, and SA of Int-PtNiN/KB at different cycle RDE test.

Cycles	$E_{1/2}$ (mV)	MA @ 0.9 V ($A\ mg_{Pt}^{-1}$)	ECSA ($m^2\ g^{-1}$)	SA @ 0.9 V ($mA\ cm^{-2}$)
0	935	1.83	62.6	2.92
10 k	932	1.63	60.7	2.69
20 k	926	1.57	59.2	2.65
30 k	924	1.33	60.3	2.21

Table S4. The half-wave potential ($E_{1/2}$), MA, ECSA, and SA of D-PtNiN/KB, D-PtNi/KB, and commercial Pt/C at different cycle RDE test.

Catalysts	Cycles	$E_{1/2}$ (mV)	MA @ 0.9 V ($A\ mg_{Pt}^{-1}$)	ECSA ($m^2\ g^{-1}$)	SA@0.9V ($mA\ cm^{-2}$)
D-PtNiN/KB	0	908	0.58	46.3	1.25
	30 k	888	0.32	40.5	0.79
D-PtNi/KB	0	890	0.46	42.0	1.10
	30k	821	0.16	34.8	0.46
Pt/C	0	850	0.18	46.6	0.39
	30 k	786	0.088	33.7	0.26

Table S5 EDX results of Int-PtNiN/KB and D-PtNiN/KB before and after 30k cycles.

		Initial		After 30k cycles	
	Element	**wt. %**	**at. %**	**wt. %**	**at. %**
Int-PtNiN/KB	**Pt**	81.6	54.7	86.1	63.0
	Ni	17.8	39.7	13.5	32.9
	N	0.6	5.6	0.4	4.1
D-PtNiN/KB	**Pt**	75.0	46.1	92.2	77.2
	Ni	24.6	50.3	7.6	21.1
	N	0.4	3.6	0.2	1.7

Table S6. Comparisons of MEA performance at a cell voltage of 0.6 V with different Pt loadings at cathodes reported in recently published papers.

	Pt loading ($mA\ cm^{-2}$)	Current density @0.6V ($mA\ cm^{-2}$)	Reference
Int-PtNiN/KB	**0.121**	**1550**	**This work**
L_{10}-CoPt/Pt	0.105	1100*	[10][10]
L_{10}-FePt/Pt	0.113	1000*	[11][11]
Pt-Ni NPs	0.1	1500*	[12][12]
PtNi-BNSs	0.15	1000	[13][13]
PtNi-BNCs	0.15	1500	[13][13]
JM 60 wt% Pt/C	0.15	800	[13][13]
JM 20 wt% Pt/C	0.1	600	[14][14]
JM 20 wt% Pt/C	0.3	724	[15][15]
Pt/C	0.2	980	[16][16]

*The data are extracted from the H_2-air fuel cell polarization curves.

Table S7. MEA test results of Int-PtNiN/KB.

Characteristic	**Units**	**Target**	**Int-PtNiN/KB**
Pt MA@0.9V	A mg_{Pt}^{-1}	> 0.44	0.49
MA loss after 30k	%	< 40	35
ECSA (H_{upd})	m^2 g^{-1}		60.9
ECSA (CO)	m^2 g^{-1}		57.4
ECSA loss (H_{upd})	%		50
ECSA loss (CO)	%		41
Voltage at 0.8 A/cm^2	mV		729
Voltage at 0.8 A/cm^2 after 30k	mV		697
Pt loading at cathode	mg cm^{-2}	< 0.125	0.121

Table S8. Coordination numbers (*N*), bond lengths (*d*), and bond length disorder parameters (σ^2) for different first nearest neighboring pairs in Int-PtNiN/KB at 0.42 V RHE determined by the EXAFS fitting shown in Figures 3c and 3d.

	N	***d* (Å)**	**σ^2 (Å^2)**
Pt-Pt	5.9 ± 0.3	2.692 ± 0.002	0.0058 ± 0.0003
Pt-Ni	3.4 ± 0.3	2.617 ± 0.003	0.0072 ± 0.0005
Ni-Ni	3.4 ±0.8	2.598 ± 0.014	0.0106 ± 0.0022
Ni-Pt	3.6 ±0.6	2.617 ± 0.003	0.0072 ± 0.0005
Ni-N	3.2 ± 0.5	2.040 ± 0.012	0.0050 ± 0.0019

The total Ni-metal (M) coordination number is 7.0 ± 1.0, which is lower than the number expected for fcc-structured single crystal cores encased by Pt shells (*N* = 12). If the interior of the core is fragmented with grain boundaries or other 2D surfaces, the coordination number would be equivalent to those of small clusters, leading to the small Ni-M coordination numbers. Dependence of coordination numbers on particle sizes is discussed in Ref [17].

Table S9. Coordination numbers (*N*), bond lengths (*d*), and bond length disorder parameters (σ^2) for different first nearest neighboring pairs in D-PtNiN/KB at 0.42 V RHE determined by the EXAFS fitting shown in Figures S14c and S14f.

	N	***d* (Å)**	**σ^2 (Å^2)**
Pt-Pt	6.0 ± 0.4	2.690 ± 0.003	0.0061 ± 0.0004
Pt-Ni	2.9 ± 0.3	2.617 ± 0.004	0.0077 ± 0.0009
Ni-Ni	3.6 ± 1.3	2.569 ± 0.030	0.0123 ± 0.0043
Ni-Pt	2.8 ± 0.8	2.617 ± 0.004	0.0077 ± 0.0009
Ni-N	4.4 ± 0.9	2.031 ± 0.020	0.0053 ± 0.0025

Table S10. The difference of Gibbs free energy (eV) and theoretical overpotential (mV) for associative 4e$^-$ pathway in Figure 4c for various tensile structures (U_{RHE}=0 V).

	0	0.2 %	0.5 %	1 %	1.5 %	2 %
ΔG_1 (eV)	-1.74	-1.72	-1.68	-1.58	-1.54	-1.99
ΔG_2 (eV)	-0.89	-0.88	-0.90	-0.98	-1.01	-1.01
ΔG_3 (eV)	-1.72	-1.55	-1.56	-1.58	-1.60	-1.61
ΔG_4 (eV)	-0.56	-0.77	-0.78	-0.77	-0.77	-0.31
η (mV)	665	**464**	**451**	**455**	**462**	923

References

(1) Sasaki, K.; Marinkovic, N.; Isaacs, H. S.; Adzic, R. R. Synchrotron-Based in Situ Characterization of Carbon-Supported Platinum and Platinum Monolayer Electrocatalysts. *ACS Catal.* **2016,** *6*, 69-76.

(2) Ravel, B.; Newville, M. ATHENA, ARTEMIS, HEPHAESTUS: data analysis for X-ray absorption spectroscopy using IFEFFIT. *J. Synchrotron Radiat.* **2005,** *12*, 537-541.

(3) Kresse, G.; Furthmuller J. Efficiency of ab-initio Total Energy Calculations for Metals and Semiconductors using a Plane-wave Basis Set. *Comput. Mater. Sci.* **1996,** *6*, 15-50.

(4) Kresse, G.; Furthmüller J. Efficient Iterative Schemes for ab initio Total-energy Calculations using a Plane-wave Basis Set. *Phy. Rev. B* **1996,** *54*, 11169.

(5) Blöchl, P. E. Projector Augmented-wave Method. *Phy.Rev. B* **1994,** *50*, 17953-17979.

(6) Perdew, J. P.; Burke, K.; Ernzerhof, M. Generalized Gradient Approximation Made Simple. *Phy. Rev. Lett.* **1996,** *77*, 3865-3868.

(7) Perdew, J. P.; Ernzerhof, M.; Burke, K. Rationale for Mixing Exact Exchange with Density Functional Approximations. *J. Chem. Phys.* **1996,** *105*, 9982-9985.

(8) Montejano-Carrizales, J.; Aguilera-Granja, F.; Moran-Lopez, J. Direct Enumeration of the Geometrical Characteristics of Clusters. *Nanostruct. Mater.* **1997,** *8*, 269-287.

(9) Marinkovic, N. S.; Sasaki, K.; Adzic, R. R. Determination of Single-and Multi-Component Nanoparticle Sizes by X-ray Absorption Spectroscopy. *J. Electrochem. Soc.* **2018,** *165*, J3222-J3230.

(10) Li, J.; Sharma, S.; Liu, X.; Pan, Y.-T.; Spendelow, J. S.; Chi, M.; Jia, Y.; Zhang, P.; Cullen, D. A.; Xi, Z.; Lin, H.; Yin, Z.; Shen, B.; Muzzio, M.; Yu, C.; Kim, Y. S.; Peterson, A. A.; More, K. L.; Zhu, H.; Sun, S. Hard-Magnet $L1_0$-CoPt Nanoparticles Advance Fuel Cell Catalysis. *Joule* **2019,** *3*, 124-135.

(11) Li, J.; Xi, Z.; Pan, Y. T.; Spendelow, J. S.; Duchesne, P. N.; Su, D.; Li, Q.; Yu, C.; Yin, Z.; Shen, B.; Kim, Y. S.; Zhang, P.; Sun, S., Fe Stabilization by Intermetallic $L1_0$-FePt and Pt Catalysis Enhancement in $L1_0$-FePt/Pt Nanoparticles for Efficient Oxygen Reduction Reaction in Fuel Cells. *J. Am. Chem. Soc.* **2018,** *140*, 2926-2932.

(12) Han, B.; Carlton, C. E.; Kongkanand, A.; Kukreja, R. S.; Theobald, B. R.; Gan, L.; O'Malley, R.; Strasser, P.; Wagner, F. T.; Shao-Horn, Y. Record Activity and Stability of Dealloyed Bimetallic Catalysts for Proton Exchange Membrane Fuel Cells. *Energy Environ. Sci.* **2015,** *8*, 258-266.

(13) Tian, X.; Zhao, X.; Su, Y.-Q.; Wang, L.; Wang, H.; Dang, D.; Chi, B.; Liu, H.; Hensen, E. J.; Lou, X.

Xia, B. Y. Engineering Bunched Pt-Ni Alloy Nanocages for Efficient Oxygen Reduction in Practical Fuel Cells. *Science* **2019,** *366*, 850-856.

(14) Ding, W.; Li, L.; Xiong, K.; Wang, Y.; Li, W.; Nie, Y.; Chen, S.; Qi, X.; Wei, Z. Shape Fixing via Salt Recrystallization: A Morphology-Controlled Approach to Convert Nanostructured Polymer to Carbon Nanomaterial as a Highly Active Catalyst for Oxygen Reduction Reaction. *J. Am. Chem. Soc.* **2015,** *137*, 5414-5420.

(15) Wang, J.; Huang, Z.; Liu, W.; Chang, C.; Tang, H.; Li, Z.; Chen, W.; Jia, C.; Yao, T.; Wei, S.; Wu, Y.; Li, Y. Design of N-coordinated Dual-Metal Sites: A Stable and Active Pt-Free Catalyst for Acidic Oxygen Reduction Reaction. *J. Am. Chem. Soc.* **2017,** *139*, 17281-17284.

(16) Fu, X.; Zamani, P.; Choi, J. Y.; Hassan, F. M.; Jiang, G.; Higgins, D. C.; Zhang, Y.; Hoque, M. A.; Chen, Z., In situ Polymer Graphenization Ingrained with Nanoporosity in a Nitrogenous Electrocatalyst Boosting the Performance of Polymer-Electrolyte-Membrane Fuel Cells. *Adv. Mater.* **2017,** *29*, 1604456.

(17) Frenkel, A. I.; Hills, C. W.; Nuzzo, R. G., A View from the Inside: Complexity in the Atomic Scale Ordering of Supported Metal Nanoparticles. *J. Phys. Chem. B.* **2001,** *105*, 12689-12703.